SUPPLEMENTARY INFORMATION

Synthesis and characterization of Cs_2TeCl_6 powder for scintillators

Lenka Prouzová Procházková,[a,b] Robert Král,[a] Mikhail G. Brik,[c,d,e] Eva Mihóková,[a] Romana Kučerková,[a] Vítězslav Jarý,[a] Vladimir Babin,[a] František Hájek,[a] Martin Nikl*[a]

[1]Institute of Physics of the Czech Academy of Sciences, Cukrovarnicka 10, 162 00 Prague, Czech Republic
[2]Czech Technical University in Prague, Faculty of Nuclear Sciences and Physical Engineering, Břehová 7, 115 19 Czech Republic
[3] School of Integrated Circuits & CQUPT-BUL Innovation Institute, Chongqing University of Posts and Telecommunications, Chongqing, 400065, China
[4]Center of Excellence for Photoconversion, Vinča Institute of Nuclear Sciences – National Institute of the Republic of Serbia, University of Belgrade, Belgrade, Serbia
[5]Institute of Physics, University of Tartu, W. Ostwald Str. 1, 50411, Tartu, Estonia

1) Structural analysis of all CTC samples

Sample 1 and 2 were prepared via procedure described in [22]. Sample 3 was prepared by simplified method – solid product was precipitated directly after mixing reaction solutions. The lattice parameters of the cubic phase as well as crystallite size *l* were determined from the observed diffraction peak positions and integral width using the Scherrer equation:

$$l = \frac{K \cdot \lambda}{\beta_{hkl} \cdot \cos\theta_{hkl}} \quad , \qquad (1)$$

where *K* is the shape factor (1.0747 for spherical particles), *λ* is the radiation wavelength and *hkl* is the integral breadth of selected diffraction line *hkl* (in radians) corrected for instrumental broadening.

Table SI1: Calculated crystallite size and lattice parameter for CTC samples no. 1,2 and 3

Sample	Crystallite size calculated from XRPD (nm)	Lattice parameter calculated from XRPD (Å)
1	524 ± 60	10.4712 ± 0.0008
2	523 ± 62	10.4662 ± 0.0018
3	524 ± 62	10.4709 ± 0.0007

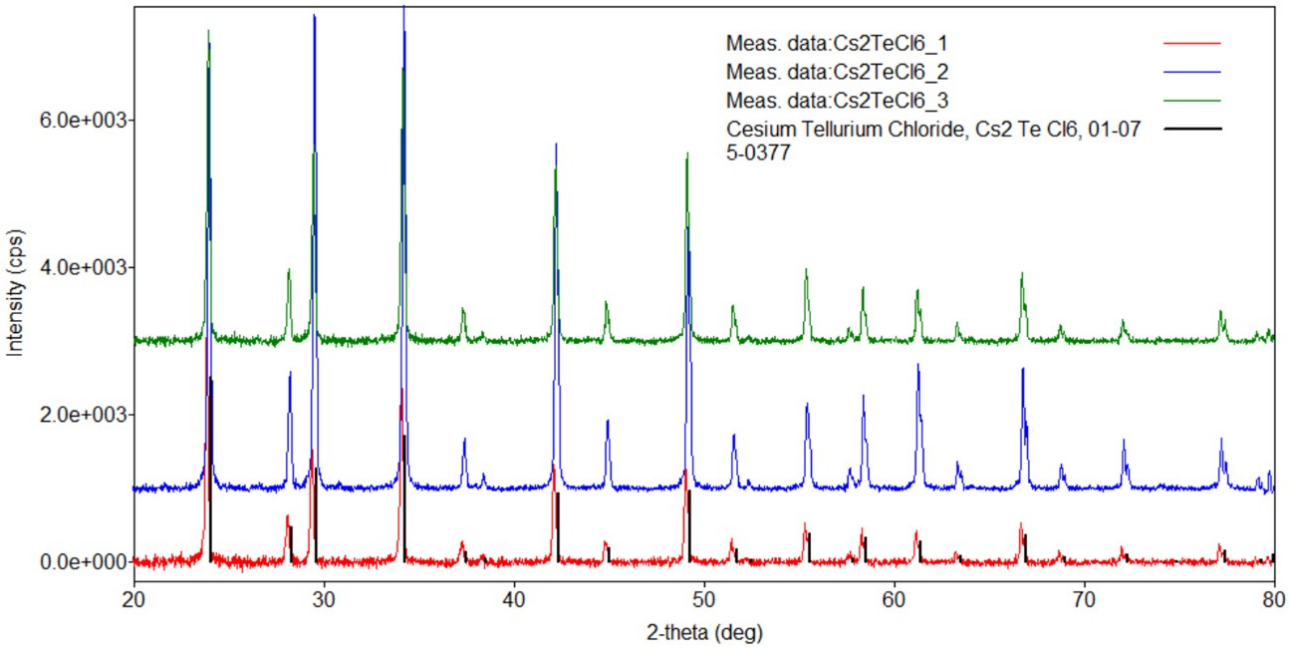

Fig. SI1: XRD data for Cs_2TeCl_6 after precipitation (Cs_2TeCl_6_2) and after hydrothermal reaction (Cs_2TeCl_6_1 and Cs_2TeCl_6_3); both phases are analyzed as a cesium tellurium chloride in the perovskite structure (#01-075-0377)

2) Phenomenological model of the temperature dependence of the PL spectra integral and PL decay times

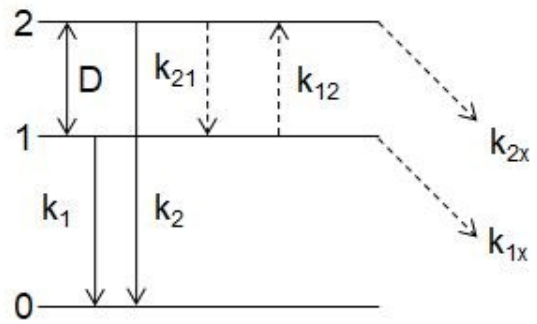

Fig. SI2: The sketch of the two excited-state-level model

The temperature dependence of both the PL decay times and PL spectra integral can be described within the two-excited-state model (schematically shown in Fig. SI2). The time evolution of the populations N_1, N_2 of the excited levels 1 and 2, respectively, can be evaluated by the following rate equations:

$$\frac{dN_1}{dt} = -k_1N_1 - k_{12}N_1 + k_{21}N_2 - k_{1x}N_1 \qquad (1)$$

$$\frac{dN_2}{dt} = -k_2N_2 - k_{21}N_2 + k_{12}N_1 - k_{2x}N_2 \ ,$$

where k_1, k_2, k_{12}, k_{21}, and $k_{1(2)x}$ are radiative transition rates from levels 1,2, non-radiative rates of phonon assisted transitions between the radiative level 2 and metastable level 1 and the quenching

channel from the level 1(2), respectively. Non-radiative transitions between levels 1,2 can be written as:

$$k_{21} = K(n+1),\ k_{12} = Kn,$$

$$n = {}^{1}/_{[\exp\left({}^{D}/_{k_B T}\right) - 1]}\ . \qquad (2)$$

Here *K, n, D* are the zero-temperature transition rate between the levels 1 and 2, the Bose-Einstein factor and energy spacing between the levels, respectively. Non-radiative quenching channel is considered in the usual barrier form:

$$k_{1(2)x} = K_{1(2)x}\left(-\frac{E_{1(2)x}}{k_B T}\right) \qquad (3)$$

with $K_{1(2)x}$ being a frequency factor and $E_{1(2)x}$ the height of the barrier. Fit of the model to the data allowed determination of characteristic parameters reported in Fig. 8.

3) Radioluminescence of CTC compared to BGO scintillation standard

Radioluminescence spectra under X-rays were measured in reflection geometry in absolute comparison with powdered BGO in Fig. SI3. BGO was used as a reference scintillation material. We integrated the peak area (480-730 nm for CTC and 330-750 nm for BGO) and compared the values for each sample prepared with BGO. From normalized values, very approximatively, considering light yield of BGO 8000-9000 phot/MeV, the value for the best CTC_3 is about 1400 phot/MeV which, however, will be lowered by lower energy depozit in CTC in comparably thick (cca 500 micrometers) pressed powder pellets due to lower effective atomic number and density of CTC (Z_{eff} = 47, ρ = 3.42 g/cm^3) compared to BGO (Z_{eff} = 74, ρ = 7.12 g/cm^3) and limited thickness of the layer from which the scintillation light can be effectively out-bound towards photodetector. Precise measurement of light yield of CTC, however, was not in the scope of this study.

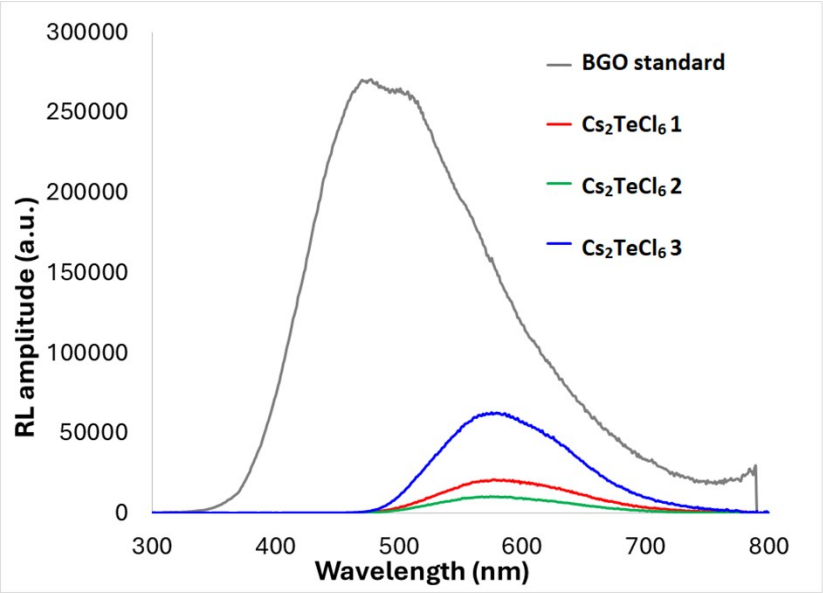

Fig. SI3: RL emission spectra for Cs_2TeCl_6 after hydrothermal reaction – experiment 1 (Cs_2TeCl_6 1), after precipitation (Cs_2TeCl_6 2) and after hydrothermal reaction – experiment 2 (Cs_2TeCl_6 3); comparison with the BGO standard

Table SI2: Emission maxima and peak area for the CTC samples and BGO strandard. Normalized values compared to BGO are in parenthesis.

Sample	Emission maximum	Peak area
1	576 nm	2735084 (0.05)
2	574 nm	1300040 (0.03)
3	575 nm	8141818 (0.16)
BGO	477 nm	50199886 (1)

4) PL decays – temperature dependence

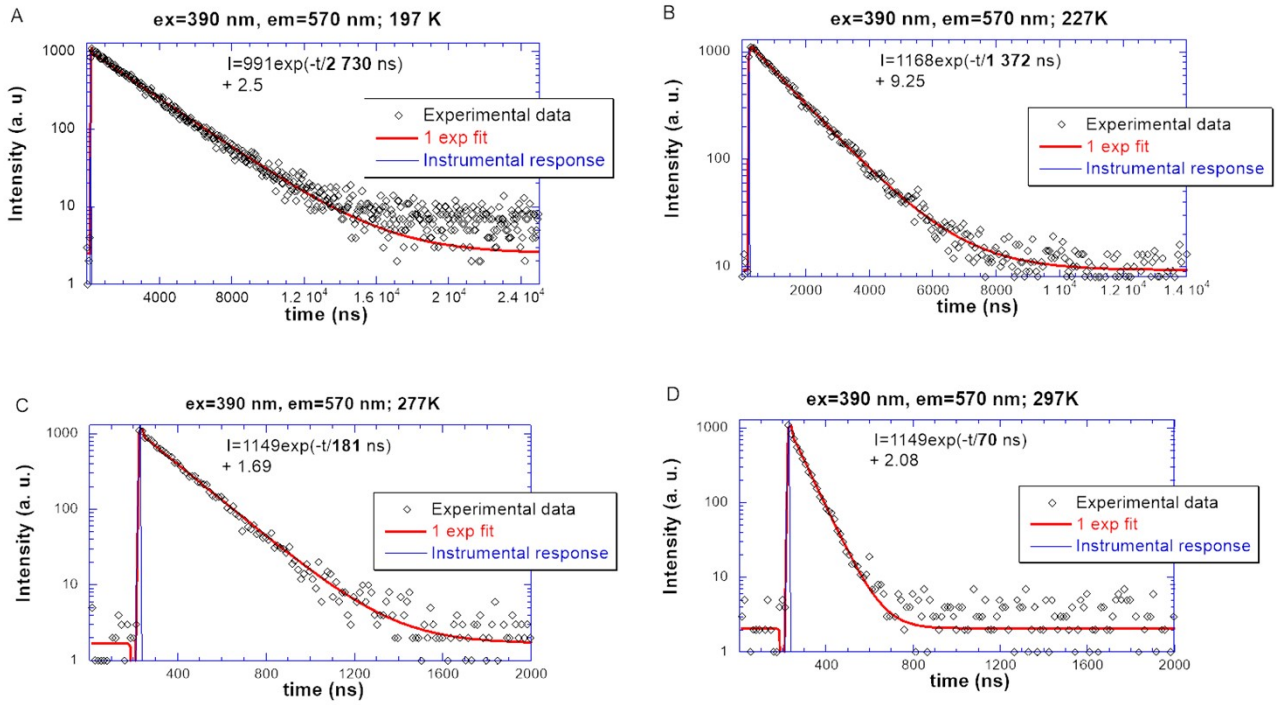

Fig. SI4: (a-d) PL decay curves (ex=390nm, em=570nm) at 197 K (a), 227 K (b), 277 K (c) and 297 K (d) approximated by a single exponential function I(t). Red line is a convolution of instrumental response and the function I(t).